

## Effects of Thermo-Mechanical Processing on the Microstructure and Mechanical Properties of $\beta$ -Type Titanium Alloys

Hakan YILMAZER <sup>1</sup> , Muhammed Enes İLGAZI <sup>1</sup> 

<sup>1</sup>*Yıldız Technical University (YTU), Faculty of Chemistry and Metallurgy, Department of Metallurgical and Materials Engineering, Istanbul, Türkiye*

### Abstract

This study investigates the microstructural evolution and mechanical behavior of severe cold-rolled  $\beta$ -type Ti-29Nb-13Ta-4.6Zr (TNTZ) alloys under systematic solution heat treatments (ST) at 1063°K for durations ranging from 5 to 60 minutes. This comprehensive analysis provides valuable insights into the microstructural and mechanical characteristics of TNTZ alloys under varying solution heat treatment durations, offering a foundational understanding for optimizing their application in engineering contexts. Microstructural analysis reveals that both solution-treated (ST) and cold-rolled (CR) samples exhibit a predominant single body-centered cubic (BCC)  $\beta$  phase, while cold-rolled and solution-treated (CST-Q) samples display a combination of  $\beta$  and martensite orthorhombic  $\alpha''$  phases. ST samples demonstrate equiaxed grains with an average diameter of  $\sim 72 \mu\text{m}$ , albeit with limited clarity. In contrast, CST-Q samples treated for over 10 minutes exhibit finer equiaxed grains within the 7-14  $\mu\text{m}$  range. Hardness values increase with prolonged solution heat treatment, reaching approximately  $\sim 183 \text{ HV}$  for ST and  $\sim 234 \text{ HV}$  for CR. Moreover, hardness continues to rise with increasing treatment duration, reaching  $\sim 204 \text{ HV}$  for CST10Q,  $\sim 229 \text{ HV}$  for CST30Q, and  $\sim 242 \text{ HV}$  for CST60Q. Mechanical properties, including tensile strength, yield strength, and elongation, vary across samples. ST shows values of  $\sim 710 \text{ MPa}$ ,  $\sim 610 \text{ MPa}$ , and  $\sim 25\%$ , CR with  $\sim 1305 \text{ MPa}$ ,  $\sim 395 \text{ MPa}$ , and  $\sim 17.5\%$ , CST5Q with  $\sim 1042 \text{ MPa}$ ,  $\sim 440 \text{ MPa}$ , and  $17.5\%$ , CST10Q with  $\sim 1010 \text{ MPa}$ ,  $\sim 650 \text{ MPa}$ , and  $21\%$ , and CST60Q with  $\sim 930 \text{ MPa}$ ,  $\sim 660 \text{ MPa}$ , and  $\sim 21\%$ . Fracture surfaces of all samples exhibit dimple structures and microvoid nucleation, indicative of ductile failure.

**Keywords:** Titanium alloys, Thermomechanical processing, Heat treatments, Mechanical properties.

### I. INTRODUCTION

Titanium (Ti) alloys find extensive application in the aircraft and bioimplant sectors owing to their superior resistance against corrosion and high specific strength.[1-5] Beta ( $\beta$ )-type Ti alloys having body centered cubic (BCC) structure are considered the most versatile group due to their remarkable combination of strength, toughness, and resistance to fatigue.[4] The  $\beta$ -type metastable Ti alloys have been advanced to enhance the mechanical behaviors of  $\beta$ -type Ti alloys, including great strength, low and moderated Young's modulus, and large ductility.[6] Recent research studies have provided evidence to support the idea that metastable alloys hold great promise for marine applications due to their exceptional cold formability and relatively favorable resistance to corrosion. These advantageous properties not only enhance their long-term durability in marine environments but also offer significant advantages in terms of processing, thanks to their ease of shaping and forming.[7] Over the past decade, there has been a significant increase in the widespread adoption of  $\beta$ -type metastable Ti alloys due to their ability to simultaneously exhibit all these properties.[8] Furthermore, the heat-treatable characteristics of metastable alloys have significantly increased their utilization in a wide array of applications.[9]

The Ti-29Ta-13Nb-4.6Zr (TNTZ) alloys having sensitive the  $\beta$  stability balance which classified metastable leads to heat treatability and martensite transformations to improve static and cyclic strength, ductility, and rigidity.[10-14] Metastable phases comprise hexagonal close-packed (HCP)  $\alpha'$ , orthorhombic  $\alpha''$  and hexagonal  $\omega$  phase. Solution treatment at 1063°K following by aging processes at temperatures below 400°C lead to longer fatigue life and high strength by controlling of these precipitates and martensites.[12,13] Heat treatment is commonly employed to achieve high strength in  $\beta$ -type metastable Ti alloys. [14,15] The strengthening process utilized for  $\beta$ -type metastable Ti alloys involves the steps of solution treatment (ST) and aging treatment (AT).[15] This processes have been utilized to optimize the microstructure and phase structure, leading to improved mechanical properties.[8] The application of ST and AT for  $\beta$ -type metastable Ti alloys can be carried out at different temperatures and durations, depending on the specific chemical composition of the alloys and the desired properties to be achieved.[16] Furthermore, severe deformed microstructure having high dislocation density leads phase transition due to the diffusion rate. The ST for  $\beta$ -type metastable Ti alloys can be conducted either in the  $\alpha/\beta$  region below the  $\beta$  transition temperature ( $T_\beta$ ) or in the  $\beta$  region at temperatures above the  $T_\beta$ . [17] The main objectives of the ST are indeed to dissolve the alloying elements into the  $\beta$  phase, create  $\beta$  phase solid solution, and achieve  $\alpha$  supersaturated  $\beta$  solid solution at room temperature. These goals are accomplished by heating the material to the  $\beta$  phase region, holding it at this temperature for  $\alpha$  suitable duration, and then rapidly quenching it to room temperature.[18]

p

This study researches into unexplored territories by investigating the profound impact of ST on both the microstructure and mechanical properties of TNTZ alloy under the rigors of severe cold rolling. What sets this research apart is the meticulous examination of phase construction, microstructural control, and mechanical properties in the context of severely deformed TNTZ. This alloy exhibits exceptional characteristics, marked by high stored energy and distortion owing to an unprecedentedly high dislocation density. The groundbreaking aspect of this study lies in

unraveling the intricate interplay between severe deformation and the resulting microstructural and mechanical transformations in TNTZ, shedding new light on materials science and engineering.

## II. MATERIALS AND METHODS

### 2.1. Materials Preparation

The present study utilized TNTZ bars having a diameter of 25 mm. The chemical composition of TNTZ is given in Table 1.

**Table 1.** Chemical composition (mass %) of the hot-forged Ti-29Nb-13Ta-4.6Zr

Ti	Nb	Ta	Zr	Fe	C	N	O	H
Bal	28.6	12.3	4.75	0.22	0.02	0.01	0.09	0.04

Figure 1 shows the sample preparation in this study. The TNTZ bars underwent a solution treatment at 1063°K for 60 minutes under vacuum conditions. Subsequently, they were quenched in iced water. The solution-treated TNTZ sample is henceforth referred to as the ST samples. The ST samples were subjected to severe cold rolling with a reduction rate of exceeding 90% to increase the density of dislocations. The cold rolled ST samples are henceforth referred to as the CR samples. The CR samples were subjected to solution treatment (ST) at 1063°K for various durations of 5, 10, 30, and 60 minutes under vacuum atmosphere. Then they are quenched in the iced water. Hereafter, these samples referred as CST-Q. The CST-Q samples were denoted as CST5Q, CST10Q, CST30Q, and CST60Q, respectively.

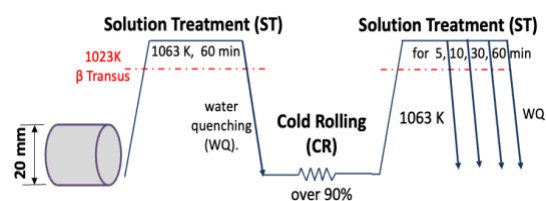


**Figure 1.** Schematic drawing of the TNTZ sample preparation.

## 2.2. Microstructural Characterization

The microstructures of the samples were examined using the metallurgical optic microscopy (OM) and X-Ray Diffraction (XRD) analysis. The specimens were prepared metallographically for the microstructural examination that their surfaces were wet grinded using the water resistant emery papers of #320- #2500 and then buff polished with the diamond solution having particles of 1  $\mu\text{m}$ . In the end, they were etched in an etching HF solution with a composition of 5% HF and 95%  $\text{H}_2\text{O}$ .

The microstructures of the samples, polished mirror like and then etched, were examined using an optical microscope integrated with a digital camera with image analysis techniques (NIS-Elements Version 4.3). The average grain diameters of the samples were calculated according to ASTM E112.

The phase constructions of the samples having a wet polished surface were characterized by X-ray diffraction (XRD, Bruker Discovery D8) with a  $\text{Cu-K}\alpha$  radiation at 40 kV and 40 mA. Diffraction patterns were acquired using a continuous scanning mode with a scan step of 0.02 degrees per second spanning the  $2\theta$  range of  $30^\circ$  to  $80^\circ$ .

## 2.3. Mechanical Tests

The Vickers hardness measurements of all samples were conducted utilizing the Vickers micro hardness instrument (HVS-1000), with a load of 1000g for a dwell time of 10 seconds. The average hardness value was calculated using 10 individual measurements.

Tensile testing of the TNTZ specimens was conducted using a tensile machine (Instron-type) with a 25 kN capacity. Prior to the test, the surfaces of the TNTZ samples were wet polished using emery papers with a grid of up to #2500. Three samples with identical dimensions were prepared for each condition for the tensile testing.

Scanning electron microscopy (SEM) was used to analyze the fracture surfaces of the samples after the tensile testing by a Zeiss EVO LS 10 SEM, equipped with a field emission cathode (FEG), operating at an accelerating voltage of 7.5 Kv.

## III. RESULTS AND DISCUSSION

### 3.1. XRD Results

The microstructure of the ST sample consists of a single BCC ( $\beta$ ) structure as reported in the previous study.[19,20] Figure 2 presents the XRD profiles of various TNTZ alloys, including CR, CST5Q, CST10Q, CST30Q, and CST60Q. The relative intensities and widths of all primary and secondary peaks, calculated by OriginLab from the profiles of CR and CST-Q samples in Table 2. The CR samples also exhibits a single  $\beta$  phase, which is consistent with previous studies. [13,21] While ST samples has a strong texture of  $\beta(110)$  [13,21], CR reveals a dominant  $\beta(200)$  orientation in its microstructure.

**Table 2.** Relative intensities of  $\beta$  peaks in XRD profiles of the CR and CST-Q samples

Peaks	Sample	Angle	Intensity	FWHM	Relative Intensity
$\beta(110)$	CR	38.541	6665.575	0.947	0.272
$\beta(200)$		55.597	14112.47	1.275	0.577
$\beta(211)$		69.688	3690.023	1.089	0.151
$\beta(110)$	CST5Q	38.541	5027.88	1.072	0.247
$\beta(200)$		55.743	208.97	0.148	0.010
$\beta(211)$		69.863	10548.86	0.894	0.518
$\alpha''(022)$		55,382	1719,313	1,043	0,225
$\alpha''(113)$		70,049	2858,273	0,418	0,225
$\beta(110)$		38.541	18803.8	0.437	0.746
$\beta(200)$	CST10Q	55.743	415.898	0.204	0.016
$\beta(211)$		69.903	3397.879	1.792	0.135
$\alpha''(022)$		55,382	1719,313	0,979	0,062
$\alpha''(113)$		70,049	849,157	0,007	0,103
$\beta(110)$		38.541	16757.47	0.333	0.752
$\beta(200)$	CST30Q	55.743	987.407	0.244	0.044
$\beta(211)$		69.834	2985.02	0.526	0.134
$\alpha''(022)$		55,382	1438,585	0,600	0,070
$\alpha''(113)$		70,049	115,983	0,005	0,070
$\beta(110)$	CST60Q	38.5413	17761.49	0.358	0.788
$\beta(200)$		55.743	452.841	0.230	0.020
$\beta(211)$		69.834	2029.061	0.592	0.045
$\alpha''(022)$		55,236	1247,846	1,162	0,103
$\alpha''(113)$		70,049	1046,033	6,969	0,051

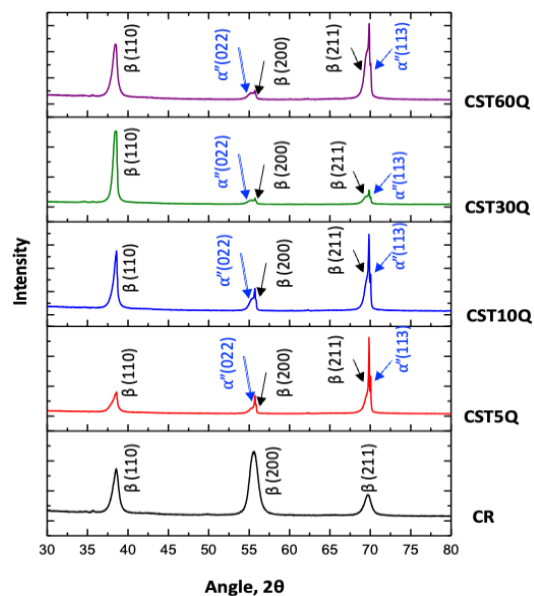


**Figure 2.** XRD profiles of the CR, CST5Q, CST10Q, CST30Q, and CST60Q sample

The results indicate a more intense  $\beta(200)$  peak on the surface during cold rolling [7], but this changes after solution treatment of CR, suggesting a change in textures due to solution treatment. Additionally, as consistent with a previous study [21], the TNTZ alloys shows stress-induced orthorhombic  $\alpha''$  martensite transformation due to their delicate  $\beta$  stability.[21]

The XRD profiles of the CST-Q samples provide evidence of the presence of martensite phase ( $\alpha''$ ) formed within the  $\beta$  matrix. The XRD patterns show the main peaks of the  $\beta$  phase, including (110), (200), and (211). After solution treatment of CR, the microstructure displays firstly a texture of  $\beta(211)$  for CST5Q. Furthermore, the  $\beta(110)$  peak exhibits a strong intensity as the treatment time increases from 10 to 60 minutes, while the relative intensity decreases.

The XRD line profile shown in Fig. 2, where the  $\beta(200)$  and  $\alpha''(022)$  peaks, as well as the  $\beta(211)$  and  $\alpha''(113)$  peaks, are distinctly observed for the solution-treated CST-Q alloys. While the initial solution treatment did not lead martensite transformation but second treatment of the severe cold rolled TNTZ microstructure shows  $\alpha''$ -martensitic transformation. It is considered that such transformation is very depending on the severe cold rolling having high dislocation density.[22]

### 3.2. Optical Micrograph

Figure 3 depicts the optical micrographs of ST and CR samples. The ST sample reveals an equiaxed coarse grains surrounding geometrical defined larger misoriented grain boundaries. Also ST grains do not show any secondary phases. The optical micrographs of CR show that the grain boundaries are not clearly visible due to severe cold rolling with a reduction ratio exceeding 90%. The microstructure exhibits a strong contrasts due to a high dislocation density along the rolling direction, making it impossible to distinguish the grain boundaries.

The optical micrographs of CST5Q, where no grain boundaries are observed, as shown in Figure 4. The microstructures of CST-Q samples shows the well-defined grains surrounding distinguishable from 10 to 60 minutes due to the increased quenching time providing sufficient duration for recrystallization.

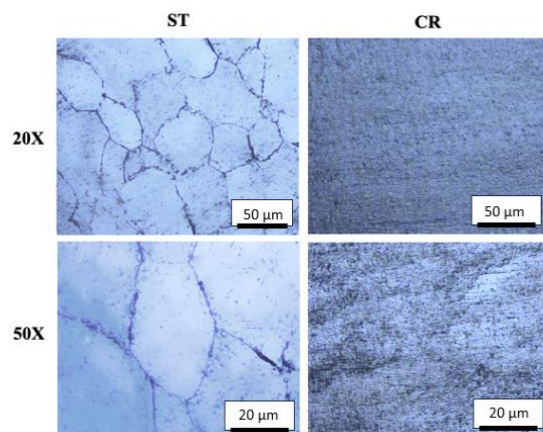


**Figure 3.** Optical micrographs of ST and CR at 20X and 50X

A result of the prolonged treatment time, allowing for further grain growth. Furthermore, the secondary  $\alpha''$  shown in the XRD profiles of the CST-Q samples does not distinguishable in the newly recrystallized grains in the optical. This results indicates. The formation of the  $\alpha''$  passes is too small to detect by Optical microscope and scanning electron microscope was reported another martensite phase hexagonal  $\omega$  phase in TNTZ.[12]

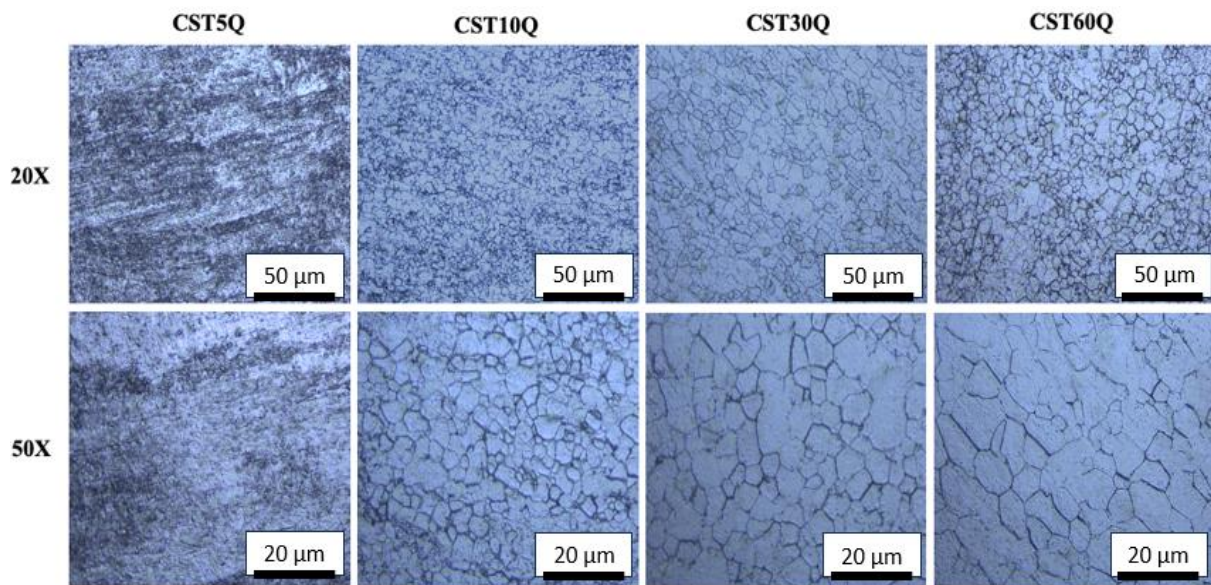


**Figure 4.** Optical micrographs of the cold rolled TNTZ subjected to solution treatment at various durations: CST5Q, CST10Q, CST30Q, and CST60Q.

Figure 5 provides an overview of the grain diameter values measured using the ImageJ application from optical micrographs of the ST, CR, CST5Q, CST10Q, CST30Q, and CST60Q. The ST sample reveals an equiaxed coarse grains having a diameter of  $\sim 72 \mu\text{m}$ . While CST5Q samples show a grain with an average diameter of around  $\sim 7 \mu\text{m}$ , the further increased treatment time increased the grain diameter to CST30Q ( $\sim 12 \mu\text{m}$ ) and CST60Q ( $\sim 14 \mu\text{m}$ ), respectively.

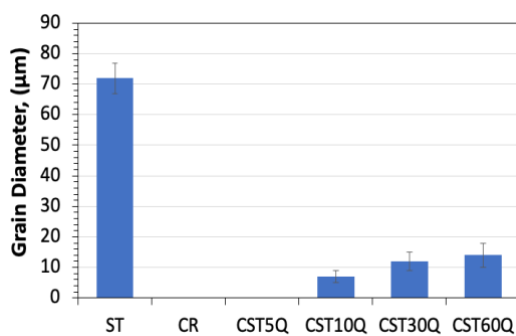


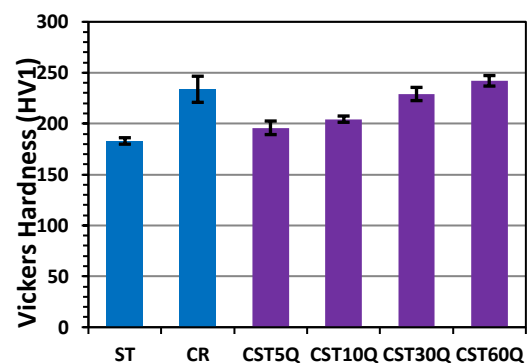
**Figure 5.** Average grain size of ST, CR, CST5Q, CST10Q, CST30Q, and CST60Q

### 3.3. Hardness Test

Figure 6 illustrates the average hardness (HV) values of the ST, CR, and CST-Q samples. The hardness of CR surpasses that of ST ( $\sim 183\text{HV}$ ), with average hardness values of  $\sim 234 \text{HV}$  respectively. The hardness values of TNTZ improved with rising the

intensity and networks of dislocations by severe distortion of the cold rolling.[12,20]

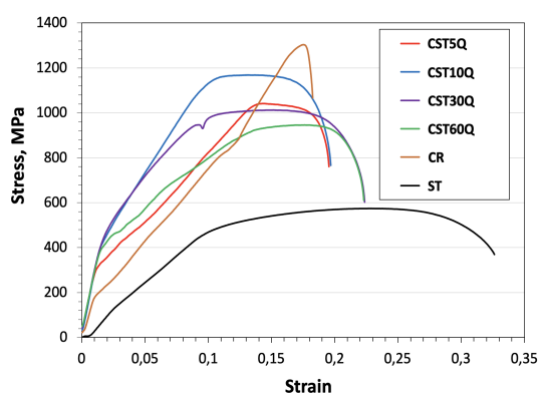
Upon solution treatment followed by ice-water quenching after severe cold rolling, the hardness of CST5Q experiences a significant decrease to  $\sim 196 \text{HV}$ , dislocation recovery and partial recrystallization.[23] The solution treatment after cold rolling leads to a gradual increase in the hardness values of TNTZ with an increase in the duration of the solution treatment due to the martensite phases.[24] The HV values are,  $\sim 204 \text{HV}$  for CST10Q,  $\sim 229 \text{HV}$  for CST30Q, and  $\sim 242 \text{HV}$  for CST60Q, respectively.



**Figure 6.** Average Vickers hardness values of the ST, CR, and CST-Q samples

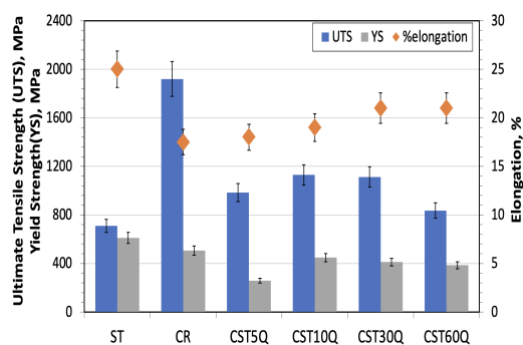
### 3.4. Tensile Strength

Figure 7 depict the stress-strain curves obtained from tensile tests of all TNTZ samples. Each stress-strain curve exhibits a distinct shape. According to the curves in the elastic regions of the stress-strain curves, the CR and CST-Q samples show similar elasticity. It is considered that the CR samples have both  $\beta$  and  $\alpha'$  phases which it was reported about the stress induced martensite transformation.[12]



**Figure 7.** Stress-strain curves of the ST, CR, CSTQ samples after tensile tests.

Figure 8 shows the mechanical properties measured by tensile tests of all TNTZ samples. While the ST samples show lowest UTS and YS values ( $\sim 710$  and  $\sim 610$  MPa) and largest elongation% ( $\sim 25\%$ ) until rupture, the CR samples shows highest UTS ( $\sim 1305$  MPa) and lowest (17,5%). The highest difference between YS and UTS indicated the strain hardening for the CR sample.[13]



**Figure 8.** Mechanical properties measured by tensile tests of the ST, CR, CST5Q, CST10Q, CST30Q, and CST60Q.

The stress-strain curves of CST-Q samples indicates CST-Q samples have higher elasticity comparing those of ST and CR due to the martensite phase. CST10Q samples exhibits an highest YS of  $\sim 670$  MPa and an UTS of  $\sim 1129$  MPa among CST-Q samples. On the other hand, the CST5Q samples shows the lowest YS of  $\sim 440$  MPa but a high UTS of  $\sim 1042$  MPa. Such large differences between YS and UTS caused by strain hardening due to the high dislocation and martensite phase. Furthermore, while CST30Q has a UTS of  $\sim 1010$  MPa and a YS of  $\sim 650$  MPa, the CST60Q has a UTS of  $\sim 930$  MPa and a YS of  $\sim 660$  MPa. They show the largest elongation of  $\sim 21\%$  among the CST-Q samples.

The SEM fractography observations of the tensile tested samples in Figure 9 and Figure 10 indicates that all fractures exhibit ductile behavior. The CR fractographs show smaller dimples than those of CST-Q samples and micro voids on the surface of the fracture. The various sizes of dimples and void nucleations are observed on the CST5Q fracture due to the undefined grain boundaries in the middle of recovery and starting recrystallization proses.[25] Similarly, with increasing solution treatment duration, the dimples in CST-Q appear to be more uniform, and the tearing ridges are wider and shorter. After solution treatment at 30 minutes, tearing ridges are observed in both CST-Q, and they become more pronounced with an increase in solution treatment time to 60 minutes.

At high magnification, voids and deep fractures are visible. The elongated parts in the fractographs indicate ductile fracture, and the elongation percentage under these experimental conditions was approximately 16-40%. This suggests that the fractures mainly consist of ductile fracture.

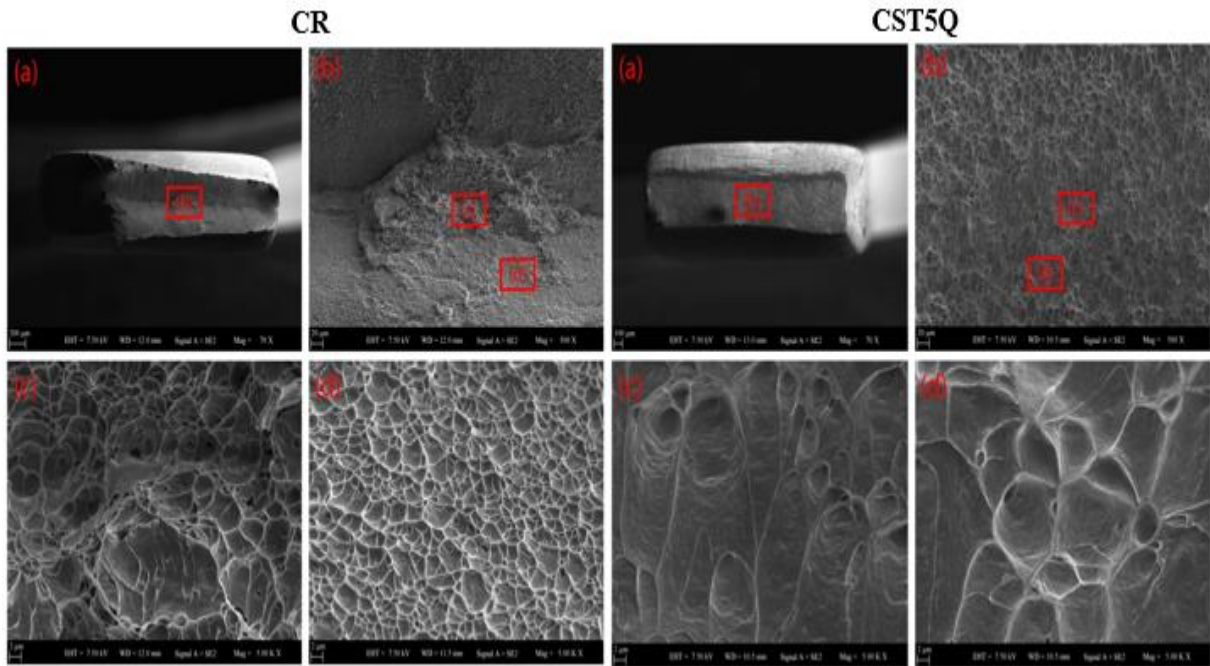


Figure 9. SEM images of the fracture surfaces of the CR and CST-5Q samples

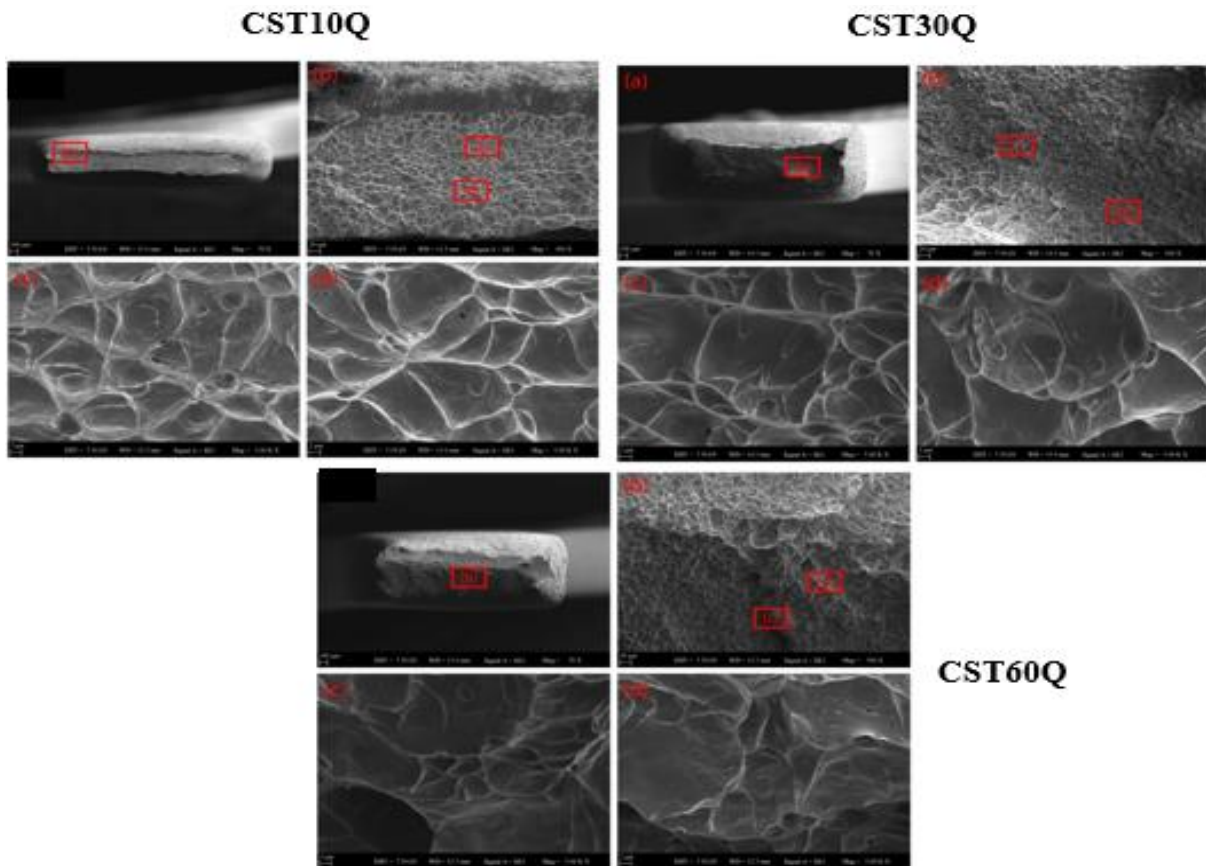


Figure 10. SEM images of the fracture surfaces of the CST-10Q, CST30Q, and CST60Q samples.

## ACKNOWLEDGEMENT

The authors would like to express great thanks to Professor Mitsuo Niinomi (Tohoku University (Sendai, Japan), (Osaka University, Osaka Japan) and Masaaki Nakai (Kindai University, Osaka, Japan) for providing hot-rolled TNTZ alloys in this study.

## IV. CONCLUSION

In this study, the microstructural features and mechanical behaviors of the severe cold rolled  $\beta$ -type Ti-29Nb-13Ta-4.6Zr (TNTZ) alloys subjected to ST at 1063°K for systematical increasing duration as 5, 10, 30, and 60 minutes. The following conclusions were obtained:

1. The microstructure of ST and CR samples consists of a single BCC ( $\beta$ ) phase. The microstructure of CST-Q samples have  $\beta$  and martensite orthorhombic  $\alpha'$  phases. While the microstructure of ST have an equiaxed grains having 72  $\mu\text{m}$ ., the grains has not been shown clearly. Also, the microstructures of CST-Q at over 10 min show equiaxed grains having diameters 7-14  $\mu\text{m}$ .
2. The hardness values of ST and CR are ~183HV and ~234 HV, respectively. In addition, the HV values are, ~204 HV for CST10Q, ~229 HV for CST30Q, and ~242 HV for CST60Q, respectively.
3. The tensile, yield strengths and elongation(%) values of the TNTZ samples are are ~710 MPa, ~610 MPa, 25% for ST; ~1305 MPa, ~395 MPa, 17.5% for CR; ~1042 MPa, ~ 440 MPa, and 17.5% for CST5Q, ~1010 MPa, ~ 650 MPa, 21% for CST10Q, for CST30Q,; and ~930 MPa, ~ 660 MPa, 21% for CST60Q.
4. In the scanning electron microscopy (SEM) images observed subsequent to the application of tensile tests, a dimple structure and micro-voids are discernible throughout the entirety of the fractured surfaces

## V. REFERENCES

[1] Long, M., & Rack, H. J. (1998). Titanium alloys in total joint replacement: A materials science perspective. *Biomaterials*, 19(18), 1621-1639. [https://doi.org/10.1016/0921-5093\(96\)10243-4](https://doi.org/10.1016/0921-5093(96)10243-4).

[2] Welsch, G., Boyer, R., & Collings, E. W. (1994). *Materials properties handbook: Titanium alloys* (1st ed.). ASM International.

[3] Singh, P., Pungotra, H., & Kalsi, N. S. (2017). On the characteristics of titanium alloys for aircraft applications. *Materials Today: Proceedings*, 4(8), 8971-8982.

<https://doi.org/10.1016/j.matpr.2017.07.249>

[4] Leyens, C., & Peters, M. (2003). *Titanium and titanium alloys: fundamentals and applications*. John Wiley and Sons. <https://doi.org/10.1002/3527602119>

[5] Lütjering, G., & Williams, J. C. (2000). *Titanium* (2nd ed.). Springer: Berlin, Germany.

[6] Pesode, P., & Barve, S. (2023). A review—metastable  $\beta$  titanium alloy for biomedical applications. *Biomedical Journal*, 46(3), 123-129. <https://doi.org/10.1016/j.bj.2023.07.001>

[7] Lan, C., Wu, Y., Guo, L., & Chen, F. (2017). Effects of cold rolling on microstructure, texture evolution and mechanical properties of Ti-32.5Nb-6.8Zr-2.7Sn-0.3O alloy for biomedical applications. *Materials Science and Engineering: A*, 690, 170-176. <https://doi.org/10.1016/j.msea.2017.02.045>

[8] Cotton, J. D., Briggs, R. D., Boyer, R. R., Tamirisakandala, S., Russo, P., Shchetnikov, N., et al. (2015). State of the art in beta titanium alloys for airframe applications. *JOM (J Occup Med)*, 67, 1281-1303. <https://doi.org/10.1007/s11837-015-1442-4>

[9] Yumak, N. & Kayali, Y. (2022). Effect of Aging Applied with the Ultra-Low Heating Rate after CRYO Treatment on the Corrosion Resistance of Metastable  $\beta$  Titanium Alloy's. *Physics of Metals and Metallography*, 14. <https://doi.org/10.1134/s0031918x22100052>

[10] Niinomi, M. (2002). Recent metallic materials for biomedical applications. *Metallurgical and materials transactions A*, 33(3), 477-486. <https://doi.org/10.1007/s11661-002-0109-2>

[11] Niinomi, M., Hattori, T., Morikawa, K., Kasuga, T., Suzuki, A., Fukui, H., & Niwa, S. (2002). Development of low rigidity  $\beta$ -type titanium alloy for biomedical applications. *Materials Transactions*, 43(12), 2970-2977.

[12] Nakai, M., Niinomi, M., & Oneda, T. (2012). Improvement in fatigue strength of biomedical  $\beta$ -type Ti-Nb-Ta-Zr alloy while maintaining low Young's modulus through optimizing  $\omega$ -phase precipitation. *Metallurgical and Materials Transactions A*, 43A, 294-302. <https://doi.org/10.1007/s11661-011-0860-3>

[13] Yilmazer, H., Niinomi, M., Nakai, M., Hieda, J., Todaka, Y., Akahori, T., & Miyazaki, T. (2012). Heterogeneous structure and mechanical hardness of biomedical  $\beta$ -type Ti-29Nb-13Ta-4.6Zr subjected to high-pressure torsion. *Journal of the Mechanical*

Behavior of Biomedical Materials, 10, 235-245. <https://doi.org/10.1016/j.jmbbm.2012.02.022>

[14] Kumar, G.L.G.S.B.S., Chinara, S., Sreetam, D., Tiwari, C., & Prakash, R. G.V.S. N. (2019). Studies on Ti-29Nb-13Ta-4.6Zr alloy for use as a prospective biomaterial. *Materials Today: Proceedings*, 15(1), 11-20.

[15] Yumak, N., Aslantaş, K. (2020). A review on heat treatment efficiency in metastable  $\beta$  titanium alloys: the role of treatment process and parameters. *Journal of Materials Research and Technology*, 9(6), 15360-15380. <https://doi.org/10.1016/j.msea.2018.03.003>

[16] Srinivasu, G., Natraj, Y., Bhattacharjee, A., Nandy, T. K., & Rao, G. V. S. N. (2013). Tensile and fracture toughness of high strength  $\beta$  Titanium alloy, Ti-10V-2Fe-3Al, as a function of rolling and solution treatment temperatures. *Materials & Design*, 47, 323-330. <https://doi.org/10.1016/j.matdes.2012.11.053>.

[17] Kolli, R., & Devaraj, A. (2018). A review of metastable beta titanium alloys. *Metals (Basel)*, 8, 506. <https://doi.org/10.3390/met8070506>

[18] Kirthika, A. M. A., Rao, M. N., & Manivasagam, G. (2022). Duplex aging of metastable beta titanium alloys: A Review. *Transactions of the Indian Institute of Metals*, 75(12), 2985-2996. <https://doi.org/10.1007/s12666-022-02696-1>.

[19] Tiyyagura, H. R., Kumari, S., Mohan, M. K., Pant, B., & Rao, M. N. (2019). Degradation behavior of metastable  $\beta$  Ti-15-3 alloy for fastener applications. *Journal of Alloys and Compounds*, 775, 518-523. <https://doi.org/10.1016/j.jallcom.2018.09.366>

[20] Yilmazer, H., Niinomi, M., Nakai, M., Hieda, J., Todaka, Y., Akahori, T., & Miyazaki, T. (2013). Mechanical properties of a medical  $\beta$ -type titanium alloy with specific micro- structural evolution through high - pressure torsion. *Materials Science and Engineering: C*, 33(5): 2499-2507. <https://doi.org/10.1016/j.msec.2013.01.056>

[21] Akahori, T., Niinomi, M., Fukui, H., Ogawa, M., & Toda, H. (2005). Improvement in fatigue characteristics of newly developed beta type titanium alloy for biomedical applications by thermo-mechanical treatments. *Materials Science and Engineering: C*, 25(3), 248-254. <https://doi.org/10.1016/j.msec.2004.12.007>

[22] Song, Z. Y., Sun, Q. Y., Xiao, L., Liu, L., & Sun, J. (2010). Effect of prestrain and aging treatment on microstructures and tensile properties of Ti-10Mo-8V-1Fe3.5Al alloy. *Materials Science and Engineering A*, 527, 691-698. <https://doi.org/10.1016/j.msea.2009.09.046>

[23] Ertorer, O., Topping, T., Lii, Y., Moss, W., & Lavernia, E.J. (2009). Enhanced tensile strength and high ductility in cry milled commercially pure titanium. *Scripta Materialia*, 60, 586-589. <https://doi.org/10.1016/j.scriptamat.2008.12.017>

[24] Jawed, S. F., Rabadia, C. D., Azim, F., & Khan, S. J. (2021). Effect of Nb on  $\beta \rightarrow \alpha''$  martensitic phase transformation and characterization of new biomedical Ti-xNb-3Fe-9Zr alloys. *Scanning*, 2021, 1-6. <https://doi.org/10.1155/2021/8173425>

[25] Bhattacharjee, A., Varma, V.K., Kamat, S.V., Gogia, A.K., & Bhargava, S. (2006). Influence of  $\beta$  grain size on tensile behavior and ductile fracture toughness of titanium alloy Ti-10V-2Fe-3Al. *Metallurgical and Materials Transactions A*, 37, 1423-1433. <https://doi.org/10.1007/s12666-008-0071-9>